Modeling cerebral blood flow velocity during orthostatic stress

Greg Mader[1], Mette Olufsen[1], Adam Mahdi[2]

(1) Department of Mathematics, NC State University, Raleigh, NC 27695, USA

(2) Institute of Biomedical Engineering, University of Oxford, Oxford, UK

ABSTRACT

Cerebral autoregulation refers to the physiological process that maintains stable cerebral blood flow during changes in arterial blood pressure. In this study, we propose a simple, nonlinear quantitative model with only four parameters that can predict cerebral blood flow velocity as a function of arterial blood pressure. The model was motivated by the viscoelastic-like behavior observed in the data collected during a postural change from sitting to standing. Qualitative testing of the model involved analysis of the dynamic responses to step-changes in pressure both within and outside the autoregulatory range, while quantitative testing was used to show that the model can fit dynamics observed in data measured from a healthy young and a healthy elderly subject. The latter involved analysis of structural and practical identifiability, sensitivity analysis, and parameter estimation. Results showed that the model is able to reproduce observed overshoot and adaptation and predict the different responses in the healthy young and the healthy elderly subject. For the healthy young subject, the overshoot was significantly more pronounced than for the elderly subject, but the recovery time was longer for the young subject. These differences resulted in different parameter values estimated using the two datasets.

Key words: Cerebral autoregulation, blood pressure, structural identifiability, practical identifiability, viscoelasticity, sensitivity analysis

INTRODUCTION

The brain accounts for only two percent of human body mass, yet approximately one fifth of the body's blood supply goes to the brain. Cerebral autoregulation (CA) is a term used to describe the brain's ability to regulate cerebral blood flow (CBF) over a wide range of blood pressures. The system works by altering the local environment, keeping the flow at homeostasis under changes in arterial blood pressure (ABP). The flow of blood to the brain is modulated both by local and global mechanisms including myogenic, metabolic, shear-dependent, and neurovascular regulation. These four regulatory responses act collectively to maintain an approximately constant CBF and oxygen supply amidst ABP changes. Myogenic regulation (33) operates by changing electrical properties of stretch-activated ion channels in arteriolar smooth muscle cells. Metabolic regulation (31) refers to the negative feedback system operating to balance metabolic demand with oxygen delivery. This response is driven by the imbalance between cerebral metabolism (demand) and oxygen delivery through CBF (supply) and acts by means of a vasoactive substance. Shear-stress regulation (35) responds to changes in wall stress imposed by changes in blood pressure and is coupled with the myogenic response. This mechanism facilitates the endothelium producing nitric oxide due to the viscous friction of blood flow along the vessel wall. Lastly, the neurogenic component of autoregulation describes the interaction between intracranial nerves and cerebral vessels (12, 33). While it has been established that these four CA mechanisms operate on different time-scales (4, 15, 32, 38) that are larger than a heart beat, the exact physiological mechanisms underlying observed dynamics are still under debate.

Generally CA is studied from two perspectives: static and dynamic. Static CA refers to the net effect a change in ABP has on CBF. It is typically illustrated by the CA curve, which is an s-shaped curve (see Figure 3) showing the range of ABP (approximately 50 to 150 mmHg) over which CBF is maintained. Outside this range CBF will change proportionally with changes in ABP. Dynamic CA refers to the time-varying response to the ABP perturbation. This is typically studied by analyzing adaptation following a step-increase in ABP. In clinical studies, an ABP change is typically induced by subjecting the patient to either postural or respiratory challenges such as head-up tilt, sit-to-stand, or CO_2 rebreathing (43).

In this study, we assess CA using data measured during postural change from sitting to standing. Upon standing, in the upper body ABP drops due to gravitational pooling, while in the lower extremities ABP increases. This leads to a decrease in cardiac output and therefore a

reduced flow to the brain. In response to this stimulus the autonomic and autoregulatory systems are activated. Baroreflex regulation restores blood pressure by regulating heart rate, cardiac contractility, and vascular tone, while CA responds via vasodilatation restoring blood flow to the brain.

Simultaneous recordings of ABP and cerebral blood flow velocity (CBFV) allow researchers to study dynamic adaptation. Figure 1 shows sample data from a sit-to-stand experiment. We note that a drop in ABP leads to an immediate drop in CBFV, which is followed by a recovery, overshoot and adaptation. This type of behavior resembles stress-strain responses observed in viscoelastic materials (10), including large arteries (42). This study develops a CA model that can predict both static and dynamic responses to changes in ABP. For changes in ABP within the CA range, the model adapts to a baseline value of CBFV, while outside the CA range changes in CBFV are proportional to ABP.

Numerous authors have tried to explain both static and dynamic aspects of CA. A variety of physiologically-based models have been proposed (32, 35, 40, 41). Ursino and Lodi used two-element (40) and three-element (39, 41) Windkessel models to predict dynamic autoregulatory responses to changes in cerebral perfusion pressure, arterial CO_2 pressure, and arterial compliance. Payne (32) proposed a lumped parameter model that relates ABP, partial CO_2 arterial pressure, and neural stimulation to predict CBF and the change in hemoglobin. Spronck et al. (35) developed a lumped parameter model that predicts static CA regulation including all four autoregulatory mechanisms. A common theme in these physiological models is that they include numerous parameters and were primarily developed to predict qualitative features rather than to fit clinical data. The physiologically-based models can be contrasted with statistical black-box approaches (7, 30). This group of methods includes the autoregulation index (ARI) (36), autoregressive-moving average (ARMA), autoregressive exogenous (ARX) (18, 19), and transfer function analysis (11, 29, 46). Although most of these methods can be used to analyze clinical data, they are rather limited in explaining physiological mechanisms underlying CA.

This study combines the two modeling methodologies deriving a simple nonlinear model that uses measured values of ABP as an input to quantitatively predict CBFV dynamics during postural change from sitting to standing. The model is motivated by the analysis of time-varying dynamics observed in the filtered and pulsatile measurements of ABP and CBFV. This analysis showed that CBFV responds nonlinearly to changes in ABP. We found it important to develop a

model that incorporates the CA curve in order to distinguish between fluctuations in ABP. Perturbations of ABP within the CA range enable CBFV to return to baseline, whereas perturbations outside this range causes CBFV to follow changes in ABP. The objective of the present study is to derive a model motivated by physiology while still keeping it as simple as possible. The latter is important since it facilitates model-based analysis of large and patient-specific ABP/CBFV datasets by comparing the estimated parameters. This type of analysis allows parameters to play the role of autoregulatory indices, which can be compared within and between groups of subjects. In this study, the model is validated using ABP/CBFV data from a representative healthy young and healthy elderly subject, but future studies aim at obtaining model parameters using data from a larger cohort of subjects. More specifically, the present study addresses data analysis, model development, and shows how stability analysis, as well as structural and practical parameter identifiability methods can be used to demonstrate that the model displays correct qualitative and quantitative behavior. Finally parameter estimation is used to show that the model can fit CBFV measurements recorded during a postural change from sitting to standing.

MATERIALS AND METHODS

Data. The sit-to-stand anonymized patient data analyzed in this paper were used with permission from Dr. Lipsitz, Hebrew SeniorLife, Boston, MA. The Institutional Review Board at Hebrew SeniorLife approved the study and all subjects provided written informed consent (17). Beat-to-beat arterial pressure was measured noninvasively in the middle cerebral artery (MCA) using a photoplethysmographic Finapres monitor (Ohmeda Monitoring Systems, Englewood, CO). The subject's nondominant hand was supported by a sling at the level of the right atrium to eliminate hydrostatic pressure effects. In order to minimize the effects of respiration, subjects were required to breathe at a rate of 15 breaths per minute with the assistance of tape-recorded cues. Test subjects also underwent Doppler ultrasonography by a trained technician in order to measure the changes in blood flow velocity within the MCA due to active postural changes. The 2 MHz probe of a portable Doppler system (MultiDop X4, DWL-Transcranial Doppler Systems Inc., Sterling, VA) was strapped over the temporal bone and locked in position with a Mueller-Moll probe fixation device to image the MCA. The MCA blood flow velocity was identified according to the criteria of Aaslid (1) and recorded at a depth of approximately 50-65 mm. The

blood flow velocity waveform, derived from a Fourier analysis of the Doppler frequency signal and continuous pressure signal, was digitized at 250 Hz and stored in the computer for later analysis.

Data processing. To inspect the trends observed in the pulsatile ABP and CBFV data, a simple filtering procedure was applied to both signals. The filtered signals $\overline{p}_a$ and $\overline{V}_{mca}$ are computed as weighted averages, where the present value is weighted higher than the past, according to the expression

$$\overline{x} = \alpha \int_{-\infty}^{t} x(s) e^{-\alpha(t-s)}\, ds, \tag{1.1}$$

where $x \in \{p_a^d, V_{mca}^d\}$ is the pulsatile data and α (1/s) represents the weighing parameter. Alternatively, differentiating equation (1.1) we obtain

$$\frac{d\overline{x}}{dt} = \alpha\left(x - \overline{x}\right). \tag{1.2}$$

In this study $\alpha = 1$ for both subjects. We note that the bigger value of α, the smoother the data is at the cost of delaying arrival of peaks and troughs. Figure 1 shows the pulsatile and filtered ABP and CBFV data for a healthy young and a healthy elderly subject. A zoom (before postural change) of the data from the elderly subject is included to show inter-beat ABP and CBFV dynamics. The black vertical lines indicate when the subjects undergo a postural change from sitting to standing, which causes the pooling of blood in the legs. As a result, the ABP in the upper body drops, while lower body ABP (not measured) increases. In response, baroreflex and autoregulation are activated, restoring ABP and CBFV to baseline levels. The young subject displays a larger overshoot before recovery than the elderly one; and the recovery time is longer in the elderly than in the young subject.

Model formulation. The proposed model is partially based on the trends observed in the filtered ABP/CBFV (input/output) data. The drop in ABP during a postural change from sitting to standing is a consequence of the blood volume redistribution triggered by gravitational forcing. Without active control systems, ABP would remain low, leading to reduced flow to the brain. While the autonomic system is activated to restore blood pressure, CA maintains CBF relatively constant. The latter is facilitated by vessel dilatation/constriction. To understand how the body adapts to these changes, it is necessary to develop a dynamic model. The data demonstrate that

the recovery time (the elapsed time between the minimum CBFV and the time at which CBFV returns to its baseline value) is longer in the elderly than in the young individual. For the young subject the recovery time is approximately 12 seconds, while it is 15 seconds for the elderly subject (see Figure 1). Conversely, the overshoot in the CBFV dynamics is larger in the young than in the elderly subject. Unfortunately, from the data used in this study it is not possible to determine what physical properties cause a larger overshoot in the young subject.

As noted earlier, the relationship between ABP and CBFV closely resembles strain-stress responses observed in viscoelastic-type materials (see (6, 9, 22, 42)), including overshoot, adaptation, and a phase shift. It is well-known that blood vessels exhibit viscoelastic properties (10). Moreover, cerebral arteries responsible for regulating CBF contain collagen and the regulatory deformation is likely to be viscoelastic. The model developed in this study is empirical and we do not have data at intermediate stages to determine exactly what type of viscoelastic response is exhibited. In general, tissue shows a continuous relaxation in response to stress (10), yet our previous study (23) revealed that with two relaxation time-constants it is possible to fit the response to ABP changes. Inspired by these studies, we chose to use the model depicted in Figure 2, which includes two Voigt bodies connected with a spring. Further, we will show how the model's parameters can be related to features associated with the adaptation, recovery, and overshoot. It should be noted that this study only accounts for the CA response due to changes in pressure. The stimulus (see Figure 2) is denoted by f_s, which represents either mean or pulsatile ABP. Numerous studies (e.g. (3, 12, 44) have attempted to predict the myogenic contribution to CA as a function of ABP, yet it is still unclear if CA responds to changes in mean or pulsatile pressure. To study the difference between these inputs, we consider two cases. The first case uses pulsatile pressure obtained via interpolating the measured ABP, i.e. $f_s = p_a^d$, and the second case explores the mean pressure stimulus predicted by interpolating the filtered pressure $f_s = \overline{p}_a$. To simplify notation in the remainder of this manuscript, we write $f_s = p$, where $p \in \{p_a^d, \overline{p}_a\}$.

The dynamic component of CA described above, predicts the transient response of CBFV to beat-to-beat fluctuations in ABP. Without any further model components CBFV would adapt to zero rather than to the given baseline flow. Therefore, to account for both dynamic adaptation

and baseline flow, we assume that V_{mca}, representing CBFV in the middle cerebral artery, is given by

$$V_{mca} = V_{dyn} + V_{bas}, \tag{1.3}$$

where V_{dyn} models the transient character of the signal and V_{bas} is the baseline value of CBFV. The dynamic portion of CBFV is predicted by determining the strain-stress relationship on each mechanical element in the model (see Figure 2). Let ε_j and σ_j for $j = 0,\ 1,\ 2$ be the strain and stress associated with the spring and the two Voigt bodies. Following the diagram in Figure 2, we can write:

$$\begin{aligned} \varepsilon_0 &= f_s - v_1 \qquad & \sigma_0 &= k_{aut}\left(f_s - v_1\right) \\ \varepsilon_1 &= v_1 - v_2 \qquad & \sigma_1 &= k_1\left(v_1 - v_2\right) + b_1\left(\frac{dv_1}{dt} - \frac{dv_2}{dt}\right) \\ \varepsilon_2 &= v_2 \qquad & \sigma_2 &= k_2 v_2 + b_2\frac{dv_2}{dt}. \end{aligned} \tag{1.4}$$

To incorporate the CA curve into our model, the spring k_2 is assumed to be a function of ABP, i.e. $k_2 = k_2(p)$. Since the two Voigt bodies and a spring are connected in series, the total stress equals to the stress on each element (6), i.e. $\sigma_0 = \sigma_1$ and $\sigma_0 = \sigma_2$, yielding

$$\begin{aligned} k_{aut}\left(f_s - v_1\right) &= k_1\left(v_1 - v_2\right) + b_1\left(\frac{dv_1}{dt} - \frac{dv_2}{dt}\right) \\ k_{aut}\left(f_s - v_1\right) &= k_2 v_2 + b_2\frac{dv_2}{dt}. \end{aligned} \tag{1.5}$$

By making the following substitutions

$$a = \frac{k_{aut}}{b_1},\ b = \frac{k_{aut}}{b_2},\ c = \frac{k_1}{b_1},\ d = \frac{k_2}{b_2}, \tag{1.6}$$

we obtain a simplified system of equations of the form

$$\begin{aligned} \frac{dv_1}{dt} &= -\left(a + b + c\right)v_1 + \left(c - d\right)v_2 + \left(a + b\right)f_s \\ \frac{dv_2}{dt} &= -bv_1 - dv_2 + bf_s, \end{aligned} \tag{1.7}$$

where a, b and c are nonnegative parameters, while d includes the pressure-dependent resistance, $k_2(p)$, used to discriminate between pressure stimuli both within and outside the CA range. Initial values for a, b, and c were chosen to ensure that the eigenvalues of the system

are negative, thereby ensuring adaptation to baseline flow. Finally, the dynamic (transient) autoregulation component of the blood flow velocity within the MCA is given by

$$V_{dyn} = M(f_s - v_1), \tag{1.8}$$

where $M \approx 1$, representing the amplification. It was noted that $d(p)$ was modeled to distinguish between pressures within and outside the CA range. Figure 3 shows a normalized pressure-flow data sets from rats (8, 13) and cats (20, 21); and a CA curve (solid line), which was modeled using a cubic polynomial of the form

$$f_{aut}(p) = 2.03 \cdot 10^{-6} p^3 - 6.02 \cdot 10^{-4} p^2 + 5.94 \cdot 10^{-2} p - 1.95. \tag{1.9}$$

It is known that the CA range is modulated in disease, e.g., hypertension (34, 37). By incorporating the steady-state expression for v_1 into equation (1.8), we obtain

$$d(p) = \frac{b\ c\ f_{aut}}{M\ c\ f_s - (a+c) f_{aut}}, \tag{1.10}$$

ensuring that at the steady-state $V_{dyn} = f_{aut}$. Moreover, it should be noted that within the auto-regulatory range $f_{aut} \approx 0$ and as a result $d \approx 0$. The CA curve is determined *a priori*, and therefore no parameters are added to the final model. Using the first "steady" portion of the subject-specific data set (before standing) and denoted by V_{mca}^d, we compute the baseline value of the CBFV as

$$V_{bas} = \frac{1}{T} \int_0^T V_{mca}^d \, dt, \tag{1.11}$$

where $T = 50$ is the length of the considered interval (in seconds). The values of V_{bas} for the young and elderly subjects have been estimated to be 57.4 cm/s and 37.7 cm/s, respectively. By combining the dynamic V_{dyn} and the baseline V_{bas}, the CBFV in the middle cerebral artery is predicted using equation (1.3). In summary, the proposed model uses ABP as an input f_s to predict CBFV during postural changes from sitting to standing.

Steady-state and initial conditions. The model is formulated as a system of two algebraic and ordinary differential equations in v_1 and v_2. To solve this system, appropriate initial conditions must be determined by, e.g., analyzing steady-state behavior within the model. We assume a

constant input stimulus $\overline{f}_s = \overline{p}$, where $\overline{p}$ is the mean pressure over the "steady" portion of the data (e.g. during sitting). Thus, the steady-state of (1.7) is given by

$$v_1^* = \frac{\overline{f}_s(bc+ad)}{bc+(a+c)d},\ v_2^* = \frac{bc\overline{f}_s}{bc+(a+c)d}, \tag{1.12}$$

where d is evaluated at $p = \overline{p}$. From this we get $V_{mca} = V_{bas} + M\left(\overline{f}_s - v_1^*\right)$. It should be noted that additional forcing is incorporated in d representing the pressure-dependent spring. However, at rest (before postural change), perturbations in pressure are assumed to be within the CA range. Given that the CA curve was normalized around zero during rest, the input stimulus is $f_{aut} = 0$, which implies that $v_1^* = v_2^* = \overline{f}_s$. One consequence of this assumption is that for simulations examining dynamics outside the CA range f_s will no longer be constant.

Time-constants. Time-constants associated with the model equation (1.7) were computed to further analyze dynamics around the nominal values of the parameters a, b and c. Since the eigenvalues λ_1, λ_2 of the Jacobian associated with system (1.7), for a constant stimulus $\overline{f}_s$, are given by

$$\lambda_{1,2} = \frac{1}{2}\left(-a-b-c-d \pm \sqrt{(a+b+c+d)^2 - 4(bc+(a+c)d)}\right), \tag{1.13}$$

where d is evaluated at $p = \overline{p}$, the time-constants of system of equations (1.7) are $\tau_{1,2} = 1/\lambda_{1,2}$. Recall that $d(p)$ is not a parameter but a pressure dependent function. We assume that CBFV returns to its baseline value after approximately 20 seconds, in agreement with the sit-to-stand data analyzed in this study (see Figure 1). To facilitate this adaptation, we impose the condition for the steady-state (1.12) to be locally stable, i.e. we require that the eigenvalues (1.13) be negative. This condition is used as a criterion for choosing the initial values (before optimization) for the parameters a, b and c. For this study it is assumed that $a = 0.25$, $b = 0.1$, and $c = 0.9$. Moreover, assuming that CA operates on more than one time-scale, we checked that optimized parameters generate two distinct time constants, $|\tau_1| \gg |\tau_2|$, which reflect the fast and slow components of the CA dynamics.

Structural identifiability. As a preliminary step for studying the model's ability to fit measured data, we consider the structural identifiability problem. It addresses the question of whether it is possible to uniquely infer the model parameters given perfect and noise-free data. If possible, structural identifiability should be considered before the practical one. Recall that the practical identifiability establishes if the model parameters can be determined uniquely given a specific (noisy) dataset. Thus, structural identifiability is a necessary condition for practical identifiability. If a model is unidentifiable, the parameters can take an infinite number of values and still produce the same response (24).

Now, we consider the structural identifiability problem for the CA model given in (1.3,1.7-1.11), assuming that ABP is within the autoregulatory range, i.e. $f_{aut} = 0$ and consequently $d = 0$, see equation (1.10). Note that under this assumption, system (1.3,1.7-1.11) reduces to two linear differential equations. As discussed in (22), the structural identifiability of the model given by equations (1.4) can be established by computing the input/output equation. To check the structural identifiability of the model (1.3,1.7-1.11), we compute the input/output equation, that is, the equation relating p with V_{mca}. First, we differentiate equation (1.3), and replace dv_1/dt with the expression in equation (1.7). Next v_1 is extracted from equation (1.3) and substituted into the current expression in equation (1.14). Finally, differentiating the resulting expression, replacing dv_2/dt with the equivalent expression in (1.7), and collecting similar terms yields the following input/output equation

$$M\frac{d^2p}{dt^2} + Mc\frac{dp}{dt} = \frac{d^2V_{mca}}{dt^2} + (a+b+c)\frac{dV_{mca}}{dt} + bc\left(V_{mca} - V_{bas}\right). \tag{1.14}$$

The structural identifiability is determined by whether the corresponding coefficient map

$$\phi(a,\, b,\, c,\, M) = \left[M,\, Mc,\, a+b+c,\, bc\right] \tag{1.15}$$

is one-to-one. It is straightforward to see that equation $\phi(a,b,c,M) = \phi(a^*,b^*,c^*,M^*)$ has a unique solution, and thus the model is structurally identifiable in the variables a, b, c, and M.

The above analysis assumed that $f_{aut} = 0$, but this is not the case in general. However, if f_{aut} is approximated by a piecewise linear functions, the model can be analyzed in its entirety. For example, if we assume that $f_{aut} = kp$, for some suitable value of k, it can be shown that the model given by (1.3,1.7-1.11) is structurally identifiable. Unfortunately, it is rather tedious to

check the property for the full nonlinear model (1.3,1.7-1.11), i.e. when f_{aut} is not necessarily assumed to be identically zero but given by equation (1.9). Thus, to analyze the ability of the general model to fit the data, the sensitivity and practical identifiability problem is considered in the following section.

Sensitivity and practical identifiability. Practical identifiability can be determined by considering the sensitivity matrix. To define sensitivities, we assume that the model can be written as

$$\begin{aligned} \frac{dv}{dt} &= f(t,v;\theta), \\ h(t;\theta) &= g(t,v;\theta), \end{aligned} \tag{1.16}$$

where t denotes time, v represents the state vector $[v_1, v_2]$, $\theta = [a,b,c,M]$ is the parameter vector, $h(t;\theta) = V_{mca}$ is the model output, and g is an algebraic function. The model output V_{mca} defined in equation (1.3) is computed as a function of the time t, the states v, and the parameter vector θ. Each column of the sensitivity matrix,

$$S = \frac{\partial V_{mca}}{\partial \theta}, \tag{1.17}$$

is a time-varying vector that measures how sensitive the model output is to a given parameter at time t (for more details see (27)). Given that model parameters do not have the same units, sensitivities cannot easily be compared across the parameter space. To remedy this problem, the sensitivity matrix is often scaled relative to the parameter and the time-varying data. The relative sensitivity matrix is defined by

$$\tilde{S} = \frac{\partial V_{mca}}{\partial \theta} \frac{\theta}{V_{mca}}. \tag{1.18}$$

As noted above, the sensitivities are functions of time for each parameter. For the purpose of parameter identification, it is useful to be able to rank the parameters according to their sensitivity. Insensitive parameters are typically not identifiable. Several measures can be used to obtain ranked sensitivities, but in this study, they are predicted by imposing a two-norm on each column of the sensitivity matrix

$$\overline{S}_i = \left|\left|S_i\right|\right|_2 . \tag{1.19}$$

Plots of the relative (time-varying) and ranked sensitivities (scaled such that the most sensitive parameter has sensitivity equal to one) for the model parameters are shown in Figure 4. Note that M is the most sensitive model parameter, while a and c are the least sensitive. For model outputs predicted numerically, parameters for which the ranked sensitivity $S_{\theta i} < \sqrt{\xi}$, where ξ is the tolerance of the ODE solver, are insensitive. For this study, the ODEs were solved numerically using Matlab's ODE solver "ode15s" with absolute and relative error set at $1 \cdot 10^{-8}$. Thus, according to the definition above, all parameters are "sensitive".

A correlation analysis was performed to explore possible pairwise correlations among the sensitive model parameters (25). The correlation matrix c can be computed from the covariance matrix $C = (S^T S)^{-1}$, as

$$c_{i,j} = \frac{C_{i,j}}{\sqrt{C_{i,i} C_{j,j}}}. \tag{1.20}$$

The matrix c is symmetric with $|c_{i,j}| \le 1$ and all $|c_{i,i}| = 1$. Here, we denote the parameter pairs for which $|c_{i,j}| > 0.95$ as correlated. By this definition, all the model parameters are practically identifiable.

Parameter estimation. The model was fit to data minimizing the least squares error

$$J = \frac{1}{N} \sum_{i=1}^{N} \left(\frac{\overline{V}_{mca}^{d}(t_i) - V_{mca}(t_i, \theta)}{V_{mca}^{d}(t_i)} \right)^2, \tag{1.21}$$

where $\overline{V}_{mca}^{d}$ denotes the filtered CBFV data, and V_{mca} is the model output. For each dataset, the parameters were estimated (see Table 1) using the Levenberg-Marquardt method (14) with nominal values $a = 0.25,\ b = 0.1,\ c = 0.9,$ and $M = 1$.

RESULTS

Qualitative results. The qualitative responses of the model (equations (1.3,1.7-1.11)) to pressure step-stimuli within and outside the CA range are presented in Figure 5. Input pressures outside of the CA range are denoted by an "**o**". The upper and the lower panels of the figure show the filtered and the pulsatile response, respectively. Figures 5A and 5D show that a step-increase in the input pressure p within the autoregulatory range (solid line) results in an initial overshoot

followed by adaptation to the same baseline value. On the other hand, a step-increase in ABP outside the CA range (dotted line) results in V_{mca} settling to a new, higher steady-state value. This is a consequence of incorporating the CA curve into the model. Similarly, the qualitative response of V_{mca} to a pressure step-decrease results in V_{mca} settling at lower CBFV value. Motivated by the sit-to-stand experiment, Figures 5C and 5F show the model's response to a "dip" in ABP. Results for this stimulus show that the model is able to predict the overshoot and baseline CBFV values recorded before the sit-to-stand protocol. Given that *in vivo* blood pressure is always pulsatile, we tested that the model could also reproduce correct behavior when responding to a pulsatile stimulus.

Quantitative responses. Figure 6 shows the model output V_{mca} (equation (1.3)) plotted against the pulsatile and filtered ABP/CBFV data from the healthy young and elderly subjects. For both subjects, the fits were generated using the optimal parameter values given in Table 1. The rightmost column shows a zoom of the steady-state segment of the data and the model response. Results obtained using the filtered ABP signal as an input show that the model is able to fit the baseline, dip, overshoot, and adaptation for both the young and elderly subjects. These three features are also captured in the model results computed using the pulsatile ABP data as a stimulus. Though it should be noted that for both the young and the elderly subjects, the model does not fully predict the widening effect portrayed by the data shortly following the transition from sitting to standing. Data for the young subject showed larger overshoot following the ABP stimulus, while the recovery time was larger for the elderly subjects. Both features can be seen in simulation results, in particular for the study using filtered ABP as an input, it should be noted that the stimulus differs between the healthy young and the healthy elderly. The comparison of estimated model parameters shows clear differences. While the parameter M is of the same order of magnitude for both subjects, the Voigt body parameters representing time-scales vary significantly between the two subject types.

DISCUSSION

This study developed a simple nonlinear model using ABP as an input to predict CBFV and analyzed the model's dynamics using both synthetic (pulsatile and non-pulsatile) and experimental data from a healthy young and a healthy elderly subject. Results showed that the

model is able to capture the CBFV drop, overshoot, and recovery, including both the more pronounced overshoot exhibited by the young subject and the longer time for recovery exhibited by the elderly subject. The model has only four parameters and was motivated by the viscoelastic-like response observed in the data recorded during postural change from sitting to standing. Comparison of estimated model parameters showed that the Voigt body parameters a, b, and c were significantly higher for the elderly subject, while M was similar for both subjects. Given that simulations were performed using one subject in each age group, statistical comparison of values is not feasible. Assuming that all other model parameters are held at their nominal values, increasing a or b results in a smaller CBFV drop and overshoot, while increasing M produces a more pronounced drop and overshoot. The model response is insensitive to changes in c (see Figure 4). Moreover, increasing a results in a longer recovery time. The higher values of a and b in aging could explain observed differences.

One noticeable discrepancy between the fits using pulsatile ABP as an input is that for the young subject, the estimated pulsatile CBFV does not predict the pulse widening observed immediately upon the postural change from sitting to standing. This widening is less pronounced in the elderly subject. This feature was captured in our previous, physiologically-based model (26), though it had more than 60 parameters compared to the 4 parameters in the current approach. It is likely that there may be a feature of CA that this model cannot quantify. For example, if the parameters associated with the change in vessel compliance are not necessarily constant, then they could be determined as a function of strain. More discussion about changes in vessel compliance with age can be found in studies by Carey et al. (5) and Yam et al. (45). Moreover, it should be noted that model simulations were performed using the same parameter set, independent of the nature of the ABP input, i.e. the model was calibrated only to the filtered and not the pulsatile response. We note that estimating parameters using the pulsatile ABP input signal did not provide a better fit.

Although the model output did not fit all aspects of pulsatile CBFV dynamics, the main features of this more complex signal were predicted well. Despite the numerous physiologically-based models that have been developed (see e.g. (32, 35, 39-41)) to our knowledge this is the first ABP/CBFV model that allows both qualitative and quantitative prediction of both the average (filtered) and transient (dynamic) responses associated with CA. The main aim of the present study was to model the transient part of ABP/CBFV response. Although the

measurements (e.g. the amplitude) of the CBFV depend on the angle of insonation, and that it may vary between individuals, it is likely that it mainly affects the scaling and not the dynamics of ABP/CBFV response.

Aside from model development, extensive model analysis was performed. To our knowledge, no previous CA models have been analyzed whether or not estimated parameters were identifiable. This question is particularly relevant if parameter values are used as physical biomarkers describing the differences both within and between groups of subjects. We showed that the linear model (when $f_{aut} = 0$) is structurally and practically identifiable. For the full nonlinear model (when $f_{aut} \neq 0$) it was not possible to show structural identifiability analytically. If the CA curve is approximated by a piecewise linear function, identifiability can be proven analytically. Regardless, subsequent sensitivity analysis showed that all model parameters were sensitive and practically identifiable allowing estimation of all model parameters. Given that the model has only four parameters, the optimizations were relatively fast. For one dataset it took approximately ten minutes using Matlab on a Macbook Pro with a 2.3 GHz Intel Core i5 processor.

While its simplicity makes the model computationally feasible to work with, it may be difficult to infer what specific physiological mechanisms were compromised. Moreover, this type of model is not yet able to predict the cause of disease, similar to many statistical methods (7, 30) and efforts aiming at computing various autoregulation indices (18, 19, 28, 36). One way to improve the current approach could be by incorporating some mechanisms present in physiologically-based models, at the same time keeping it computationally efficient. Several previous aprroaches could be used as a point of departure for this effort including the works by Ursino et al. (40, 41), Arciero et al. (2) or Spronck et al. (35), which quantify in detail the metabolic, myogenic, shear-dependent, and neurogenic responses. The advantage of the latter models is that they can be used to understand how each mechanism impacts the overall dynamics, a feature not provided by our study. The disadvantage is the high number of parameters, which are typically unidentifiable, making the model difficult to validate against experimental data.

In conclusion, the CA model developed in this study is able to predict both qualitative and quantitative dynamics associated with ABP/CBFV response during a postural change from

sitting to standing. Qualitative features were analyzed by imposing step-changes and a "dip" change in ABP within and outside the CA range. Quantitative responses were analyzed by showing that the model can fit both filtered and pulsatile CBFV dynamics during a postural change from sitting to standing, a feature that to our knowledge has not been tested in previous modeling studies. Parameter estimation was used to show that the model could be adapted to distinguish responses in a healthy young and healthy elderly subject. The model provided very good agreement with the data (for the subjects shown). Finally, we showed that the model exhibits an important nonlinearity related with the CA curve.

ACKNOWLEDGMENTS

The authors would like to thank the Virtual Physiological Rat (VPR) project for supporting this work under NIH-NIGMS grant 1P50-GM094503-01A0 subaward to North Carolina State University. In addition, Olufsen received partial support from the National Science Foundation under grants NSF-DMS 1122424 and NSF-DMS 0636590, and Mahdi acknowledges the partial support of the EPSRC project EP/K036157/1. This study would not have been possible without the access to anonymized patient data provided by Dr. Lewis Lipsitz at the Hebrew SeniorLife in Boston, MA. The authors would also like to thank Prof. Johnny Ottesen for reading the manuscript and offering a number of helpful comments.

REFERENCES

1. Aaslid R., K.F. Lindegaard, W. Sorteberg, and H. Nornes. Cerebral autoregulation dynamics in humans. *Stroke*. 20: 45–52, 1989.
2. Arciero J.C., B.E. Carlson, and T.W. Secomb. Theoretical model of metabolic blood flow regulation: roles of atp release by red blood cells and conducted responses. *Am. J. Physiol. Heart Circ. Physiol.* 295: H1562–H1571, 2008.
3. Bevan J.A., and J.J. Hwa. Myogenic tone and cerebral vascular autoregulation: the role of a stretch-dependent mechanism. *Ann. Biomed. Eng.* 13: 281–286, 1985.
4. Black M.A., N.T. Cable, D.H. Thijssen, and D.J. Green. Importance of measuring the time course of flow-mediated dilatation in humans. *Hypertension*. 51: 203–210, 2008.
5. Carey B.J., R.B. Panerai, and J.F. Potter. Effect of aging on dynamic cerebral autoregulation during head-up tilt. *Stroke*. 34: 1871–1875, 2003.
6. Christensen R.M. *Theory of Viscoelasticity, an Introduction.* New York: Academic Press, 1971.
7. Czosnyka M., S. Piechnik, H.K. Richards, P. Kirkpatrick, P. Smielewski, and J.D. Pickard. Contribution of mathematical modeling to the interpretation of bedside tests of cerebrovascular autoregulation. *J. Neurol. Neurosurg. Psychiatry.* 63: 721–731, 1997.
8. Dirnagl U., and W. Pulsinelli. Autoregulation of cerebral blood flow in experimental focal brain ischemia. *J. Cereb. Blood Flow Metab.* 10: 327–336, 1990.
9. Flügge W. *Viscoelasticity.* New York: Springer Verlag, 1975.
10. Fung Y.C. *Biomechanics: Mechanical properties of living tissues.* New York: Springer-Verlag, 1993.
11. Giller C.A. The frequency-dependent behavior of cerebral autoregulation. *Neurosurgery.* 27: 362–368, 1990.
12. Hamner J.W., and C.O. Tan. Relative contributions of sympathetic, cholinergic, and myogenic mechanisms to cerebral autoregulation. *Stroke*. 45: 1771–1777, 2014.
13. Harper S.L., H.G. Bohlen, and M.J. Rubin. Arterial and microvascular contributions to cerebral cortical autoregulation in rats. *Am. J. Physiol. Heart Circ. Physiol.* 246: H17–H24, 1984.
14. Kelley C.T. *Iterative methods for optimization*. Philadelphia: SIAM, 1999.

15. Lanzarone E., P. Liani, G. Baselli, and M.L. Costantino. Model of arterial tree and peripheral control for the study of physiological and assisted circulation. *Med. Eng. Phys.* 29: 542–555, 2007.
16. Lassen N.A. Cerebral blood flow and oxygen consumption in man. *Physiol. Rev.* 39: 183–238, 1959.
17. Lipsitz L.A., S. Mukai, J. Hamner, M. Gagnon, and V. Babikian. Dynamic regulation of middle cerebral artery blood flow velocity in aging and hypertension. *Stroke*. 31: 1897–1903, 2000.
18. Liu Y., and R. Allen. Analysis of dynamic cerebral autoregulation using an ARX model based on arterial blood pressure and middle cerebral artery velocity simulation. *Med. Biol. Eng. Comput.* 40: 600–605, 2002.
19. Liu Y., A.A. Birch, and R. Allen. Dynamic cerebral autoregulation assessment using an ARX model: comparative study using step response and phase shift analysis. *Med. Eng. Phys.* 25: 647–653, 2003.
20. MacKenzie E.T., J.K. Farrar, W. Fitch, D.I. Graham, P.C. Gregory, and A.M. Harper. Effects of hemorrhagic hypotension on the cerebral circulation. I. Cerebral blood flow and pial arteriolar caliber. *Stroke*. 10: 711–718, 1979.
21. MacKenzie E.T., S. Strandgaard, D.I. Graham, J.V. Jones, A.M. Harper, and J.K. Farrar. Effects of acutely induced hypertension in cats on pial arteriolar caliber, local cerebral blood flow, and the blood-brain barrier. *Circ. Res.* 39: 33–41, 1976.
22. Mahdi A., N. Meshkat, and S. Sullivant. Structural identifiability of viscoelastic mechanical systems. *PLoS One.* DOI: 10.1371/journal.pone.0086411, 2014.
23. Mahdi A., J. Sturdy, J.T. Ottesen, and M.S. Olufsen. Modeling the afferent dynamics of the baroreflex control system. *PLoS Comput. Biol.* DOI:10.1371/journal.pcbi.1003384, *2013.*
24. Meshkat N., and S. Sullivant. Identifiable reparametrizations of linear compartment models. *J. Symbolic. Comput.* 63: 46–67, 2014.
25. Miao H., X. Xia, A.S. Perelson, and H. Wu. On identifiability of nonlinear ode models and applications in viral dynamics. *SIAM Rev. Soc. Ind. Appl. Math.* 53: 3–39, 2011.

26. Olufsen M.S., J.T. Ottesen, H.T. Tran, L.M. Ellwein, L.A. Lipsitz, and V. Novak. Blood pressure and blood flow variation during postural change from sitting to standing: model development and validation. *J. Appl. Physiol.* 99: 1523–1537, 2005.
27. Olufsen M.S., and J.T. Ottesen. Patient specific parameter estimation and heart rate regulation. *J. Math. Biol.* 67: 39–68, 2013.
28. Panerai R.B., P.J. Eames, and J.F. Potter. Variability of time-domain indices of dynamic cerebral autoregulation. *Physiol. Meas.* 24: 367–381, 2003.
29. Panerai R.B., A.W.R. Kelsall, J.M. Rennie, and D.H. Evans. Analysis of cerebral blood flow autoregulation in neonates. *IEEE Trans. Biomed. Eng.* 43: 779–788, 1996.
30. Panerai R.B., A.W.R. Kelsall, J.M. Rennie, and D.H. Evans. Cerebral autoregulation dynamics in premature newborns. *Stroke*. 26: 74–80, 1995.
31. Paulson O., S. Strandgaard, and L. Edvinsson. Cerebral autoregulation. *Cerebrovasc. Brain Metab. Rev.* 2: 161–192, 1990.
32. Payne S.J. A model of the interaction between autoregulation and neural activation in the brain. *Math. Biosci.* 204: 260–281, 2006.
33. Peterson E.C., Z. Wang, and G. Britz. Regulation of cerebral blood flow. *Int. J. Vasc. Med.* DOI: 10.1155/2011/823525, 2011.
34. Serrador J.M., S.J. Wood, P.A. Picot, M.S. Kassam, R.L. Bondar, A.H. Rupert, and T.T. Schlegel. Effect of acute exposure to hypergravity (GX vs. GZ) on dynamic cerebral autoregulation. *J. Appl. Physiol.* 91: 1986–1994, 2001.
35. Spronck B., E.G. Martens, E.D. Gommer, and F.N. van de Vosse. A lumped parameter model of cerebral blood flow control combining cerebral autoregulation and neurovascular coupling. *Am. J. Physiol. Heart Circ. Physiol.* 303: H1143–H1153, 2012.
36. Tiecks F., A.R.A. Lam, and D. Newell. Comparison of static and dynamic cerebral autoregulation measurements. *Stroke*. 26: 1014–1019, 1995.
37. Tryambake D., J. He, M.J. Firbank, J.T O'Brian, A.M. Blamire, and G.A. Ford. Intensive blood pressure lowering increases cerebral blood flow in older subjects with hypertension. *Hypertension*. 61: 1309–1361, 2013.
38. Ursino M. Interaction between carotid baroregulation and the pulsating heart: a mathematical model. *Am. J. Physiol. Heart Circ. Physiol.* 44: H1733–H1747, 1998.

39. Ursino M., and C.A. Lodi. Interaction among autoregulation, CO_2 reactivity, and intracranial pressure: a mathematical model. *Am. J. Physiol. Heart Circ. Physiol.* 274: H1715–H1728, 1998.
40. Ursino M., and C.A. Lodi. A simple mathematical model of the interaction between intracranial pressure and cerebral hemodynamics. *J. App. Physiol.* 82: 1256–1269, 1997.
41. Ursino M., A. Ter Minassian, C.A. Lodi, and L. Beydon. Cerebral hemodynamics during arterial and CO_2 pressure changes: in vivo prediction by a mathematical model. *Am. J. Physiol. Heart Circ. Physiol.* 279: H2439–H2455, 2000.
42. Valdez-Jasso D., D. Bia, Y. Zocalo, R.L. Armentano, M.A. Haider, and M.S. Olufsen. Linear and nonlinear viscoelastic modeling of aorta and carotid pressure-area dynamics under in vivo and ex vivo conditions. *Ann. Biomed. Eng.* 39: 1438–1456, 2011.
43. van Beek A.H., J.A. Claassen, M.G. Rikkert, and R.W. Jansen. Cerebral autoregulation: an overview of current concepts and methodology with special focus on the elderly. *J. Cereb. Blood. Flow. Metab.* 28: 1071–1085, 2008.
44. Walsh M.P., and W.C. Cole. The role of actin filament dynamics in the myogenic response of cerebral resistance arteries. *J. Cereb. Blood Flow Metab.* 33: 1–12, 2013.
45. Yam A.T., E.W. Lang, J. Lagopoulos, K. Yip, J. Griffith, Y. Mudaliar, and N.W. Dorsch. Cerebral autoregulation and ageing. *J. Clin. Neurosci.* 12: 643–646, 2005.
46. Zhang R., J.H. Zuckerman, C.A. Giller, and B.D. Levine. Transfer function analysis of dynamic cerebral autoregulation in humans. *Am. J. Physiol. Heart Circ. Physiol.* 274: H233–H241, 1998.

TABLE

Parameter	Equation	Description	Value (Y)	Value (E)
a	(1.7)	Voigt-body parameter	0.438	2.50
b	(1.7)	Voigt-body parameter	0.0100	0.280
c	(1.7)	Voigt-body parameter	0.264	2.71
M	(1.8)	Mathematical amplifier	1.20	1.00

Table 1: Estimated model parameters and values for the healthy young (Y) and elderly (E) subjects.

FIGURE CAPTIONS

Figure 1: *Trends in ABP/CBFV dynamics*. Graphs show pulsatile and filtered ABP and CBFV data for a healthy young (left column) and a healthy elderly (middle column) subject during the sit-to-stand experiment. The black vertical lines mark the time at which the subjects stand.

Figure 2: *Mechanical analog used for predicting* V_{dyn}. Schematic diagram depicting the mechanical analog model used for predicting the dynamic CA component V_{dyn}. The model includes two viscoelastic Voigt body elements combined with a spring accounting for the elastic portion of the response. The stick figure illustrates the sit-to-stand experiment. Circles are used to mark locations at which the ABP (closed circle) and CBFV (open circle) are measured. The ABP is used as the model stimulus via f_s (closed circle), and the model output V_{dyn} (open circle) is used to estimate the patient-specific CBFV.

Figure 3: *CBF-Pressure Curve*. Empirical fit of f_{aut} against normalized experimental CBF and ABP data from rats (8, 13) and cats (20, 21). These data suggests that CA range is defined for ABP between approximately 50 and 150 mmHg.

Figure 4: *Sensitivity analysis*. This figure shows the relative (time-varying) [left panel] and ranked [right panel] sensitivities of the model parameters with respect to the model output, CBFV.

Figure 5: *Qualitative responses*. This figure presents six qualitative responses computed using the ABP/CBFV model. Simulations were done by varying the input pressure (ABP) assuming: step increases (A), step decreases (B), ABP drop followed by recovery (C), oscillating step increases (D), oscillating step decreases (E), and an oscillating ABP drop followed by recovery (F). Solid lines represent ABP changes within the CA range, and dotted lines indicate pressure changes outside of the CA range. Steps outside of the CA range are denoted by "**o**".

Figure 6: *Quantitative responses*. Estimated mean and pulsatile CBFV model output compared to filtered and pulsatile CBFV data for a young subject and an elderly subject. The vertical black line in each plot denotes the beginning of orthostatic stress.

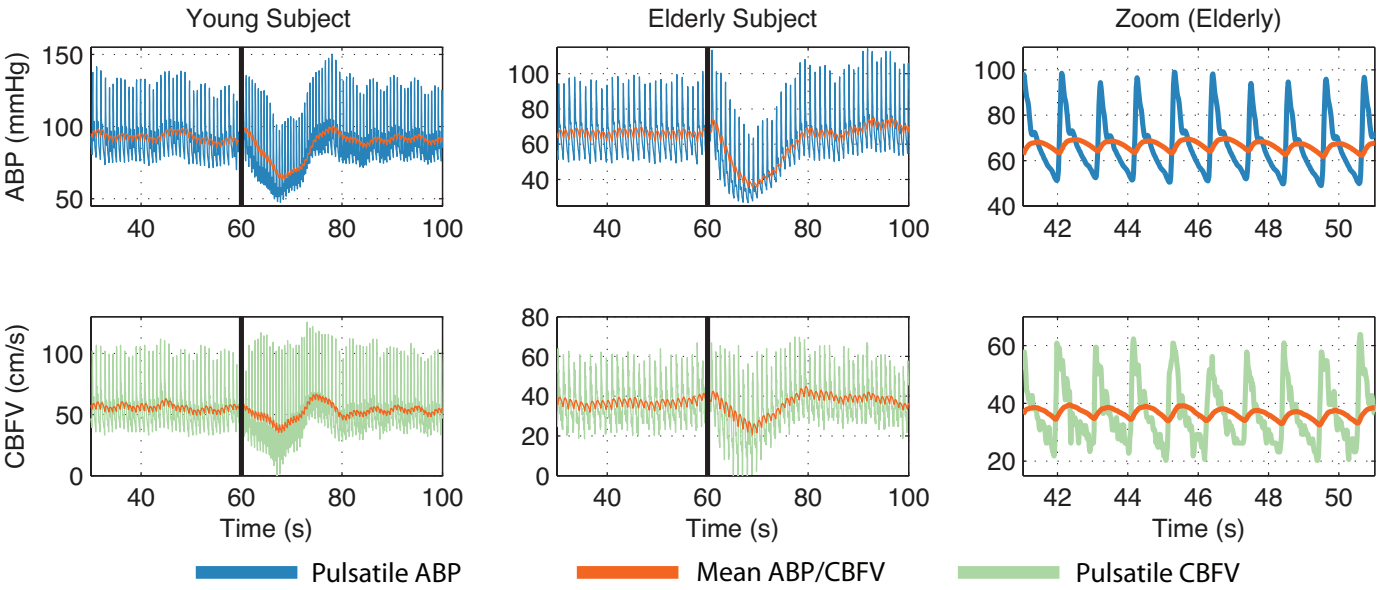

Figure 1: *Trends in ABP/CBFV dynamics*

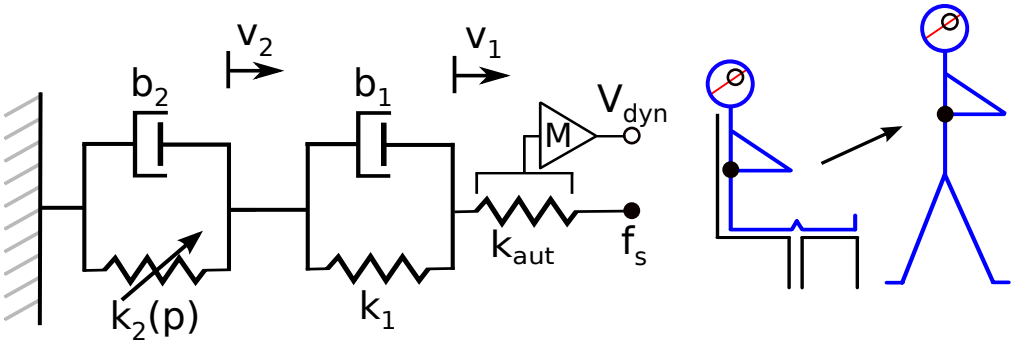

Figure 2: *Mechanical analog used for predicting* V_{dyn}

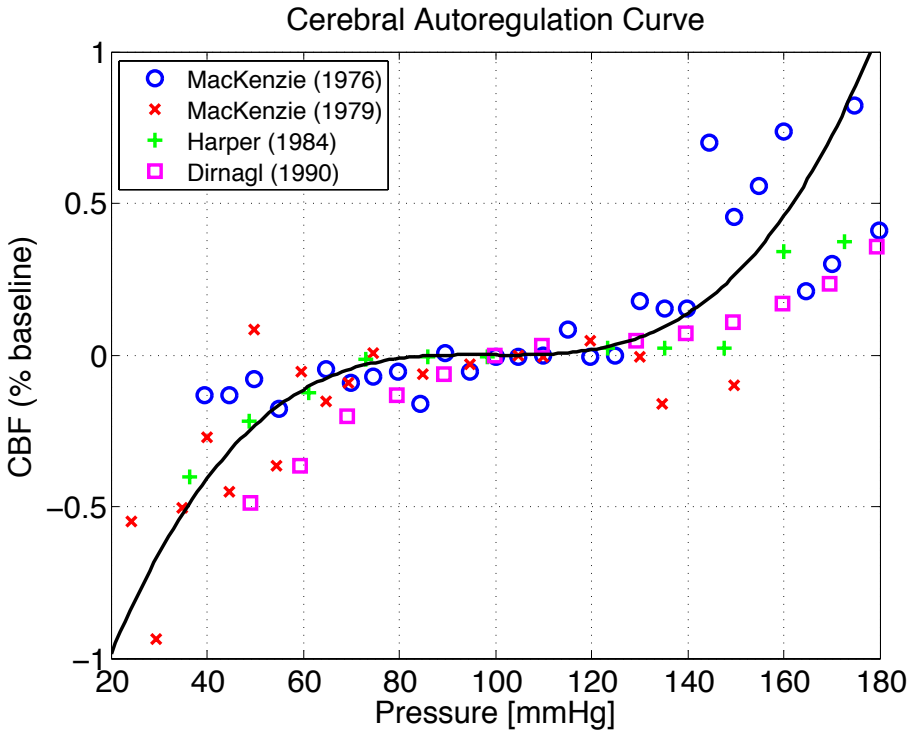

Figure 3: *CBF–Pressure Curve*

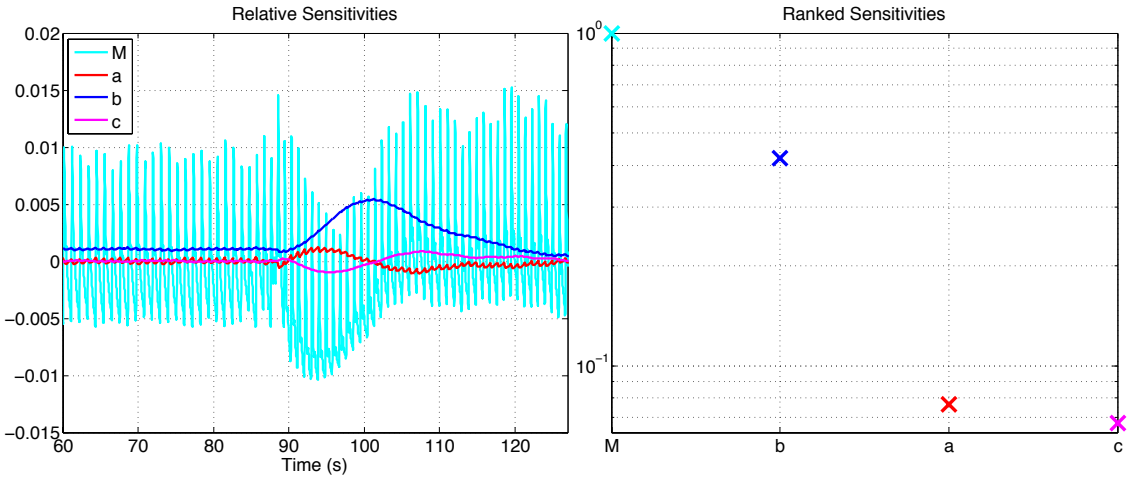

Figure 4: *Sensitivity analysis*

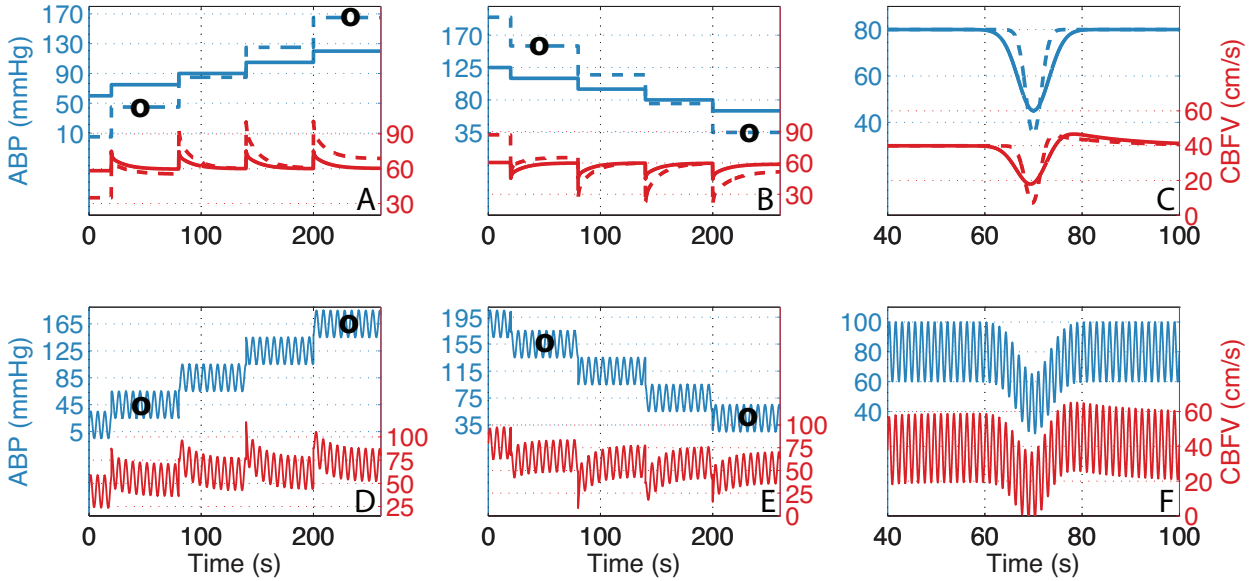

Figure 5: *Qualitative responses*

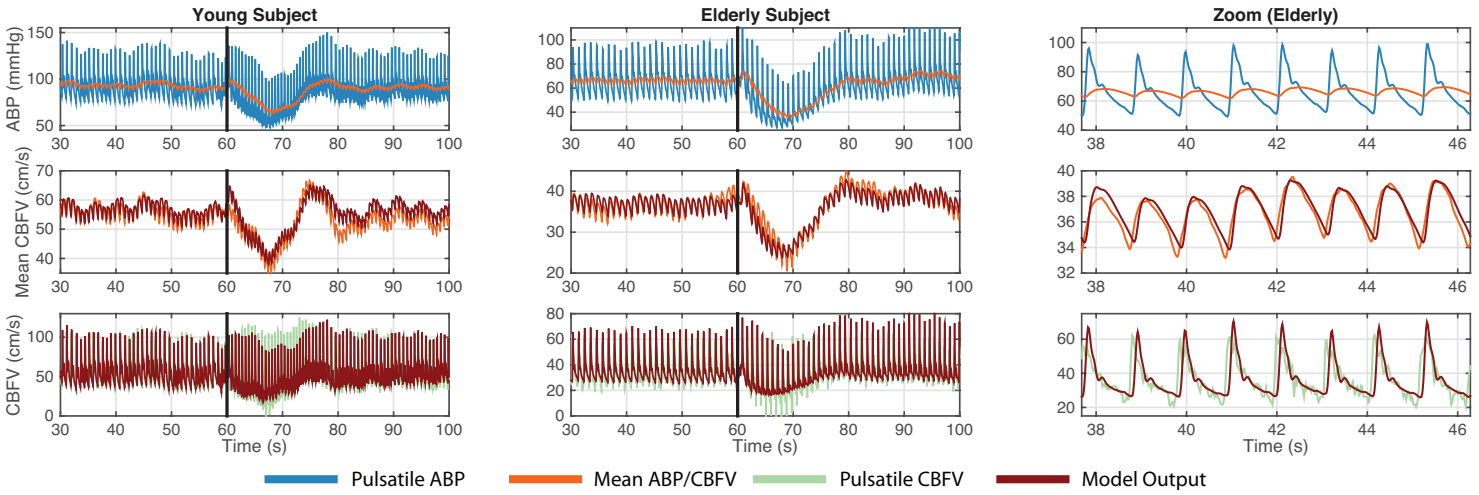

Figure 6: *Quantitative responses*